JACS
JOURNAL OF THE AMERICAN CHEMICAL SOCIETY
pubs.acs.org/JACS
Article

An Electrically Conducting Li-Ion Metal–Organic Framework

Darsi Rambabu, Alae Eddine Lakraychi, Jiande Wang, Louis Sieuw, Deepak Gupta, Petru Apostol, Géraldine Chanteux, Tom Goossens, Koen Robeyns, and Alexandru Vlad*

Cite This: *J. Am. Chem. Soc.* 2021, 143, 11641–11650
Read Online

ABSTRACT: Metal–organic frameworks (MOFs) have emerged as an important, yet highly challenging class of electrochemical energy storage materials. The chemical principles for electroactive MOFs remain, however, poorly explored because precise chemical and structural control is mandatory. For instance, no anionic MOF with a lithium cation reservoir and reversible redox (like a conventional Li-ion cathode) has been synthesized to date. Herein, we report on electrically conducting Li-ion MOF cathodes with the generic formula Li_2-**M**-DOBDC (wherein **M** = Mg^{2+} or Mn^{2+}; $DOBDC^{4-}$ = 2,5-dioxido-1,4-benzenedicarboxylate), by rational control of the ligand to transition metal stoichiometry and secondary building unit (SBU) topology in the archetypal CPO-27. The accurate chemical and structural changes not only enable reversible redox but also induce a million-fold electrical conductivity increase by virtue of efficient electronic self-exchange facilitated by mix-in redox: 10^{-7} S/cm for Li_2-**Mn**-DOBDC vs 10^{-13} S/cm for the isoreticular H_2-**Mn**-DOBDC and Li_2-**Mg**-DOBDC, or the Mn-CPO-27 compositional analogues. This particular SBU topology also considerably augments the redox potential of the $DOBDC^{4-}$ linker (from 2.4 V up to 3.2 V, vs Li^+/Li^0), a highly practical feature for Li-ion battery assembly and energy evaluation. As a particular cathode material, Li_2-**Mn**-DOBDC displays an average discharge potential of 3.2 V vs Li^+/Li^0, demonstrates excellent capacity retention over 100 cycles, while also handling fast cycling rates, inherent to the intrinsic electronic conductivity. The Li_2-**M**-DOBDC material validates the concept of reversible redox activity and electronic conductivity in MOFs by accommodating the ligand's noncoordinating redox center through composition and SBU design.

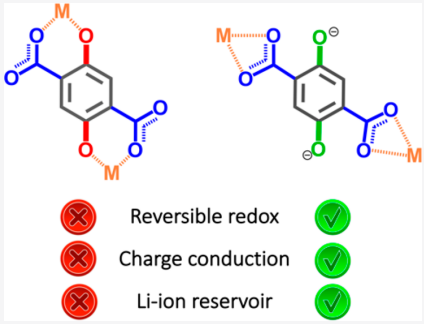

DOI : 10.1021/jacs.1c04591

An Electrically Conducting Li-ion Metal-Organic Framework

*Darsi Rambabu, Alae Eddine Lakraychi, Jiande Wang, Louis Sieuw, Deepak Gupta, Petru Apostol, Géraldine Chanteux, Tom Goossens, Koen Robeyns, and Alexandru Vlad**

Institute of Condensed Matter and Nanosciences, Université catholique de Louvain, 1348 Louvain-la-Neuve, Belgium.

**Contact author: alexandru.vlad@uclouvain.be*

KEYWORDS: Li-ion cathode; Electronic conductivity; MOF; Reversible redox; High voltage.

Abstract: Metal-Organic Frameworks (MOFs) emerge as an important, yet highly challenging class of electrochemical energy storage materials. The chemical principles for electroactive MOFs remain however poorly explored because precise chemical and structural control is mandatory. For instance, no anionic MOF with lithium cation reservoir, and reversible redox (alike a conventional Li-ion cathode) has been synthesized to date. Herein, we report on electrically conducting Li-ion MOF cathodes with the generic formula Li_2-**M**-DOBDC (wherein **M** = Mg^{2+} or Mn^{2+}; $DOBDC^{4-}$ = 2,5-dihydroxybenzene-1,4-dicarboxylate), by rational control of the ligand to transition metal stoichiometry and SBU topology in the archetypal CPO-27. The accurate chemical and structural changes not only enable reversible redox, but also induce a million-fold electrical conductivity increase by virtue of efficient electronic self-exchange facilitated by mix-in redox: 10^{-7}S/cm for Li_2-**Mn**-DOBDC *vs.* 10^{-13} S/cm for the isoreticular H_2-**Mn**-DOBDC and Li_2-**Mg**-DOBDC, or the Mn-CPO-27 compositional analogues. This particular SBU topology also considerably augments the redox potential of the $DOBDC^{4-}$ linker (from 2.4V up to 3.2V, *vs.* Li^+/Li^0), a highly practical feature for Li-ion battery assembly and energy evaluation. As a particular cathode material, Li_2-**Mn**-DOBDC displays an average discharge potential of 3.2V *vs.* Li^+/Li^0, demonstrates excellent capacity retention over 100 cycles, while also handling fast cycling rates, inherent of the intrinsic electronic conductivity. The Li_2-**M**-DOBDC material is validating the concept of reversible redox activity and electronic conductivity in MOFs by accommodating the ligand's non-coordinating redox center through composition and SBU design.

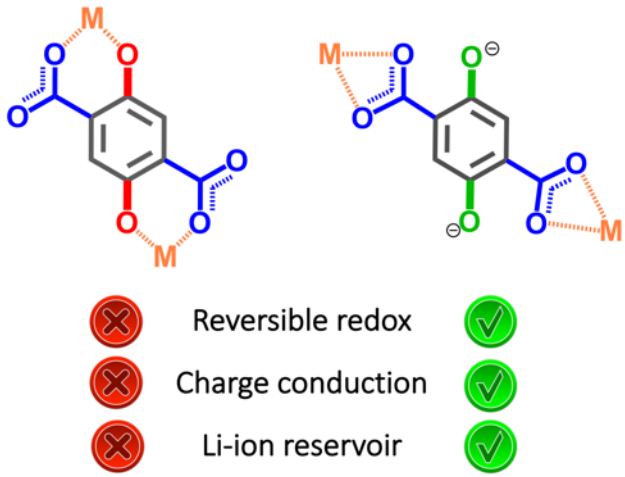

1. INTRODUCTION

Rechargeable batteries, particularly lithium-ion batteries (LIBs), appear nowadays as an essential technology to satisfy the high energy demand of our society,[1] which is steadily increasing due to continuous technological and population growth.[2] The inorganic-based electrode materials in LIBs rely on scarce elements (e.g. Cobalt), require energy consuming fabrication processes and bear recyclability issues as well as environmental burdens. These fundamental bottlenecks bring challenges related to cost, environmental footprint as well as end-of-life fate. Among many sustainable alternatives, organic electrode materials (OEMs) are emerging as promising solution to promote low-polluting and sustainable energy storage devices.[3,4,5] However, these also present a series of drawbacks such as solubility in conventional liquid electrolytes, low intrinsic electrical conductivity and low energy density metrics.

Over the past years, hybrid Metal Organic Frameworks (MOFs) have flourished as electrode materials for the next-generation electrochemical energy storage devices.[6–13,14–17] Thanks to their superior functionality, unique morphology, design flexibility and structural integrity, MOFs are capable of fitting into the required parameters for an efficient electrode material. At the material level, high gravimetric energy could be achieved thanks to the hybrid nature allowing the charge storage from both metal cations and organic ligands,[18] whereas cycling stability and facile ion transport are inherent of the polymer-like robust network and the porous structure, respectively. Additionally, MOFs with intrinsic electronic conductivity can also be designed[6,7,19] resulting in enhanced power density and allow electrode fabrication with minimum amount of conductive carbon additives. [13]

In the context of alkali-ions storage, many MOFs have been reported as both positive and negative electrode materials.[6,8,10,11,13,20] Despite high specific capacities attained, MOF-based negative electrodes (anode materials) require further improvements, and in particular to lower the redox potential, reduce the voltage hysteresis (and thus increase the energy efficiency), and augment the first cycle coulombic efficiency. MOF-based positive electrodes (cathode materials) are more challenging to design and further innovation is desired with structure-composition-property synergy between organic linkers and metal nodes. Despite the significant advances attained in this direction[21-33] (and as described in the following section), a specific class of MOF positive electrode materials is still missing from this landscape: the Li-ion MOF electrode materials with reversible redox of the anionic framework, or the metal nodes, with Li-cations contained to compensate the charge.

Herein, we report on the first generation of Li-ion MOFs with general composition of Li_2-**M**-DOBDC (**M** = Mg^{2+} or Mn^{2+}; $DOBDC^{4-}$ = 2,5-dihydroxybenzene-1,4-dicarboxylate) as a Li-reservoir positive electrode material for LIBs. The targeted MOFs are successfully synthesized, thoroughly

characterized and electrochemically evaluated. The change of metal cation and SBU node topology is found to affect drastically the redox reversibility and electronic conductivity. Another effect of the modified SBU topology is the notable increase in the redox potential value of the ligand by as much as 800 mV (as compared to free ligand, $DOBDC^{4-}$) as well as enhanced rate and cycling performances attained with 91% of the capacity preserved when cycled at a rate of 1C, and over 100 cycles for Li_2-**Mn**-DOBDC electrodes.

2. OVERVIEW OF DESIGN STRATEGIES FOR MOF-BASED POSITIVE ELECTRODE MATERIALS

Implementing MOFs as positive electrode materials for batteries remains a relatively young and uncharted area. Scheme 1 presents an overview of charge transfer pathways during redox in MOFs along with major achievements attained in this area to date. As positive electrodes we consider herein the MOF materials with an average discharge potential above 2V (*vs.* Li^+/Li^0). Distinction has to be made between *n*-type and *p*-type redox mechanism (Scheme 1 – part A) as this implies difference in nature of the stored ions (*e.g.* cations and anions, respectively) with consequence on real energy storage metrics. A sub-classification by metal redox-active combined to ligand redox-innocent MOFs (Scheme 1-B1) and ligand redox-active combined to metal redox-innocent, or mix-in redox of both ligand and metal (Scheme 1-B2) is also presented.

Tarascon and colleagues were the first to report on the integration of MIL-53(Fe) MOFs as electrode materials for energy storage.[21,22] With this specific composition, the redox-activity was limited to the transition metal center (Scheme 1-B1). Following these pioneering developments, further advances have been attained in this sub-class, with different MOF compositions and structures being tested.[21,22,23,24,25] Zhang *et al.*[27,28] and Aubrey *et al.*[32] pushed these concepts to a next level, by exploring the mix-in redox of both, metal cations and organic ligands in copper anthraquinone-dicarboxylate (Cu(2,7-AQDC)) and iron 4,4'-dioxidobiphenyl-3,3'-dicarboxylate (Fe_2(dobpdc)) MOFs, respectively (Scheme 1-B2). A major advance was achieved by the use of electrically conductive MOFs for capacitive charge storage.[13] Further discussion on redox active MOFs for charge storage is provided in SI (Section - *Overview of MOF positive electrode materials*). Overall, the redox potential and attained capacities cover a wide range, and have steadily increased since the original developments, clearly emphasizing on the rising importance of the MOF-based electrode materials for energy storage.

However, one type of MOF chemistry which is missing is that described by the anionic frameworks with charge compensating alkali metal cations that would display a reversible redox and operate according to a classical Li-ion rocking chair mechanism, preferably at a redox potential of above 3V vs. Li^+/Li^0. In their seminal work on MIT-20 MOFs, Dincă and his team have indeed prepared

alkali and alkali-earth ion doped anionic MOFs for solid-state ionic conduction applications, yet with irreversible redox.[34] With the materials and rationales presented in this work, we complement the MIT-20 family with redox reversible (and thus useful for direct charge storage) anionic Li-ion MOFs. Additionally, and opposite to MIT-20 MOFs, the Li_2-**Mn**-DOBDC MOF is an electronic conductor, a property assigned to electronic self-exchange inherent of mix-in redox of ligand and metal nodes.

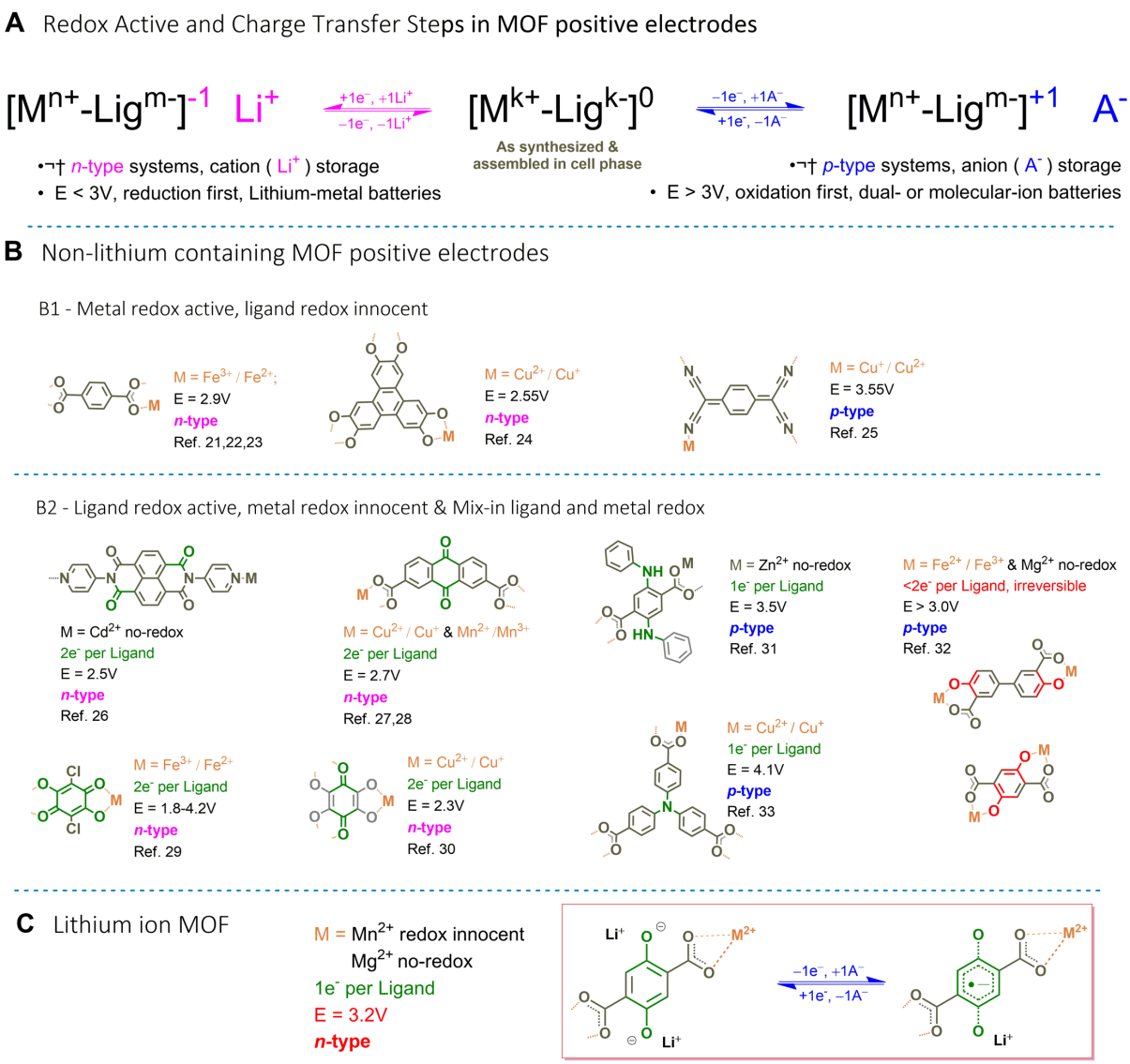

Scheme 1. Overview of possible redox mechanism and MOF classes developed and applied as positive electrode materials for electrochemical charge storage. (A) Possible charge transfer steps taking place during redox in MOFs, depending on the nature of metal centres and organic linkers. (B) Non-lithium containing vs. (C) lithium containing (reservoir) MOF battery materials. Average redox potentials are given versus Li^+/Li^0 pseudo-reference electrode.

3. RESULTS AND DISCUSSION

Our interest in DOBDC electroactive linker was triggered by a series of fundamental questions but also practical considerations (Scheme 1). On the fundamental side, the work of Aubrey *et al*.[32] aroused our interest by the fact that the reversible redox of this specific ligand could not be accessed whereas chemical oxidation seems possible, yet following different reaction pathways depending on the chemistry of the metal node: *i.e.* Fe(II) vs. Mn(II) and Mg(II).[32,35] Further, the isoreticular Fe_2(dobpdc) framework was shown to display reversible redox of two electrons relying only on the $Fe^{2+/3+}$ couple. The ligand redox was attained at much higher potential (> 4.1 V vs. Li^+/Li^0), while reported as not reversible. Given these, we presumed that the transition metal binding to the phenolate redox centers of DOBDC or DOBPDC would affect the electroactive properties, in either blocking the redox, or increasing considerably the redox potential value, given the high ionic potential of the metal node and charge depopulation of the redox center.[36] This rationale seemingly holds true for certain quinone-containing MOFs, while still not applicable to other.[37] The reversible redox was indeed found in Cu- and Mn-AQDC[27,28] with non-coordinated quinone groups (Scheme 1-B2), but also in Fe-DHBQ[29] and Cu-THQ[30] where the metal is coordinated to quinone redox centers.

The $DOBDC^{4-}$ linker is also interesting because of its low molecular mass and extensively characterized electrochemistry in solution,[38,39] and in solid-phase.[36] For MOF design, it has the interesting feature of being a tetra-anion; thus leaving space for tuning the cation composition and stoichiometry. With just two different cations, as selected here (*e.g.* Li^+ and Mn^{2+}), three different compositions can be attained: Li_4-DOBDC, Li_2-**Mn**-DOBDC and Mn_2-DOBDC. The former is a tetralithium non-porous salt, extensively studied in the organic battery community;[36,40,41,42,43] whereas the latter is the stereotypical Mn-CPO-27 MOF (or Mn-MOF-74). The intermediate one remains hitherto unexplored. This MOF composition will not only serve as a lithium reservoir electrode material, but also allow the investigation of the fundamental question on whether the phenolate binding to Mn has any effect on the redox response.

2.1. Synthesis, structural reversibility and physico-chemical analysis of Li_2-M-DOBDC MOFs

In contrast to synthesis of Li_4-DOBDC or Mn-CPO-27 that can be simply achieved by reacting equimolar amounts of Li^+ or Mn^{2+} salts and DOBDC ligand, the synthesis of Li_2-**Mn**-DOBDC is not straightforward, and applying similar synthesis conditions resulted in a mix of Li_4-DOBDC and Mn-CPO-27. We thus developed a step-wise post-synthetic MOF modification approach (Figure 1), relying on DOBDC-based MOFs with secondary building unit (SBU) formed solely by carboxylate groups (Table S1). The first step was the synthesis of H_2-**M**-DOBDC•DMF_2 (M= Mn, Mg).[44] The Mn phase is isostructural to the reported Mg analogue, and was also confirmed by single-crystal XRD analysis (refer to Experimental Section, SI). The Mn(II) nodes are coordinated octahedrally with four H_2-$DOBDC^{2-}$

linkers in the equatorial position and two DMF molecules at axial position (Figures 1 and S1a). The carboxylate groups of H_2-DOBDC^{2-} act as bidentate linkers bridging two Mn(II) nodes, forming 1D $\{Mn(CO_2)\}_n$ chains, extending in 3D space by an alternative interlinking of H_2-DOBDC^{2-} units (Figure S1b). Square-shaped channels are observed along the *a*-axis and the uncoordinated pendant phenolic –OH groups of H_2-DOBDC^{2-}are pointing inwards (Figure 1).

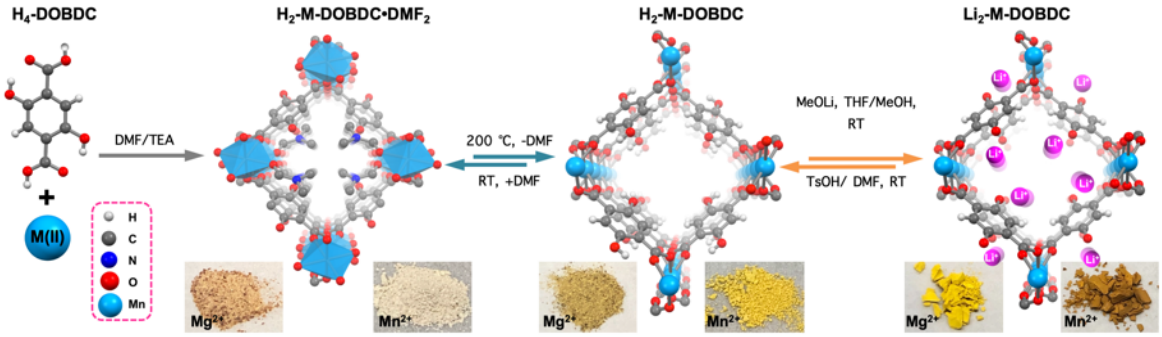

*Figure 1. Schematic view of the synthetic routes adopted for H_2-**M**-DOBDC·DMF_2, H_2-**M**-DOBDC and Li_2-**M**-DOBDC (**M** = Mn, Mg) preparation, highlighting the reversibility of the last two steps. Optical micrographs displaying the morphology and the colour of the materials in powder form for each composition.*

The essential feature of the H_2-**M**-DOBDC•DMF_2 is the uncoordinated nature of the phenolic-OH groups which leaves the opportunity for cation exchange with a lithium containing base. However, all lithiation attempts failed while working with the solvated phase, presumably due to the clogging of the pores by DMF molecules, so a desolvation step was required. According to TGA analysis (Figure S2), the desolvation of H_2-**Mn**-DOBDC·DMF_2 was achieved at 200 °C for 32h under vacuum. The desolvation process was accompanied by a pronounced colour change from pale yellow to bright yellow coloured H_2-**Mn**-DOBDC (Figure 1). PXRD revealed a phase change upon desolvation, with a shift of low angle peaks from 2θ = 9.5° and 11.8° to 2θ = 9.1° and 10.2°; suggesting the preservation of the open framework with partial disordering (Figures 2a and S3). Similarly, the desolvation of H_2-**Mg**-DOBDC·DMF_2 was achieved following the same protocol with PXRD pattern similar to the reported one.[45] The desolvated phases of H_2-**M**-DOBDC were further confirmed by FTIR analysis (Figure 2b and S4). The disappearance of the characteristic stretching vibrations of DMF ($\nu_{C=O}$, at 1654 and 1642 cm^{-1} and $\nu_{C-H}(CH_3)$ at 2934 cm^{-1}) and red shift of the carboxylate band is observed (from 1586 to 1562 cm^{-1}) due to stronger interaction between Mn(II) and carboxylate group (Figure 2b). Notably, the broad

phenolic −OH band positioned around ~3200 cm^{-1} in both H_2-**M**-DOBDC MOFs remains conserved after the desolvation, and therefore still available for the cation exchange step.

To obtain the targeted Li_2-**M**-DOBDC MOFs, the protonated versions were reacted with stoichiometric amounts of CH_3OLi under inert atmosphere, resulting in clear colour change of the powders (Figure 1). The deprotonation was confirmed by the complete disappearance of the broad phenolic-OH band along with the $\nu_{C\text{-}OH}$ deformation bands located at ~3200 cm^{-1} and 1230–1234 cm^{-1} (Figure 2b). The appearance of the $\nu_{C\text{-}OLi}$ vibration band at 1200 and 1209 cm^{-1} for Mn(II) and Mg(II) respectively, indicates formation of phenolate-OLi groups. A comparison of Li_2-**M**-DOBDC and Mn-CPO-27 IR spectra indicates that the shift of the carboxylate and the phenolate bands is significantly dependent on the ionic potentials of M(II) and SBU environment. This significantly impacts the electrochemical properties of the studied MOFs accordingly, as will also be discussed further in the electrochemical analysis section.[36] The ICP-AES analysis revealed close to expected compositions of 1:1.94 (Mn:Li) for Li_2-**Mn**-DOBDC and 1:1.89 (Mg:Li) for Li_2-**Mg**-DOBDC. TGA highlights the increased stability of the lithiated frameworks of up to 500°C, contrary to the protonated MOFs which decompose at ~250 °C (Figures S2 and S5) attributed to stronger ionic interactions of Li^+ and phenolate $–O^-$ within the framework, as also observed for Li_2(Mg)-*p*-DHT (isochemical to Li_2-**Mg**-DOBDC reported here).[36]

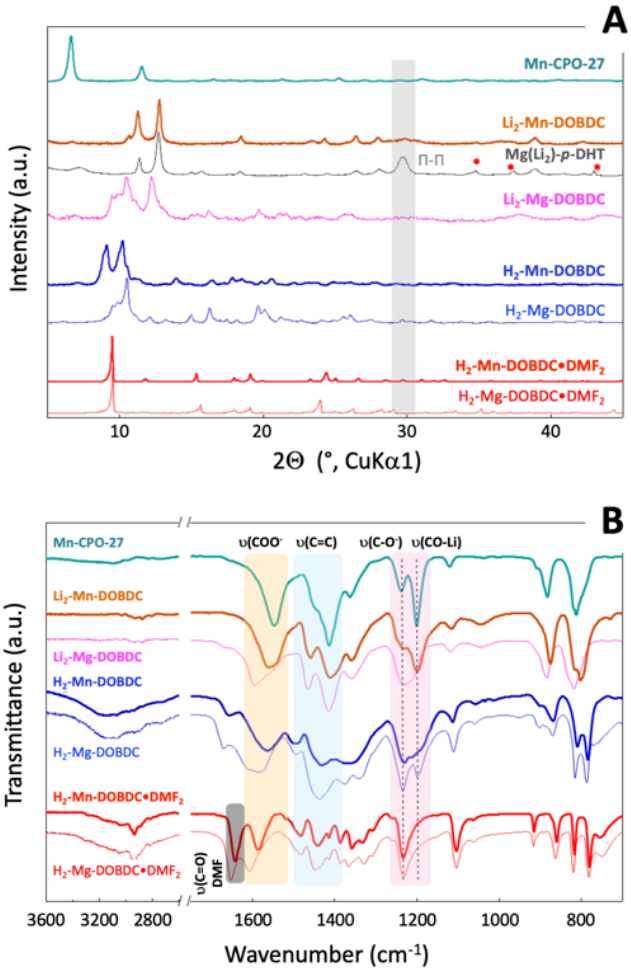

*Figure 2. Overlaid PXRD patterns (A) and FTIR spectra (B) for H_2-**M**-DOBDC·DMF_2, H_2-**M**-DOBDC, Li_2-**M**-DOBDC (**M** = Mn, Mg), synthesis intermediates and products. The data for Mn-CPO-27 and of Mg(Li_2)-p-DHT[36] phase is included for comparison. * - indicates the diffraction peaks of Al_2O_3 coming from measurement set-up background; and π-π the characteristic pi-stacking peak.*

Structural and compositional survey of the post-synthetic functionalization steps are resumed in Figure 2 (complemented by data and discussion in Figures S3, S4 and S6). Despite the similarity in the crystal structure, the pristine H_2-**M**-DOBDC•DMF_2 frameworks undergo different structural changes upon desolvation and H^+/Li^+ exchange. The quality of PXRD data was not high enough to be indexed and confirm the crystal structure of the H_2/Li_2-**M**-DOBDC phases. Nevertheless, we indirectly confirm this by chemical reversibility analyses of the H_2-**M**-DOBDC•DMF_2 - H_2-**M**-DOBDC - Li_2-**M**-DOBDC series by forward and reverse functionalization (last 2 steps in Figure 1). The same phases are obtained upon re-solvation with DMF and Li-H exchange (Figures S3, and S4). These are confirmed by the appearance/disappearance of characteristic vibration bands in FTIR (*e.g.*, $\nu_{C=O}$ for DMF and $\nu_{C\text{-}OH}$ for phenol) as well as the high similarity between PXRD pattern of pristine and processed MOFs (Figure S3 and S4).[46] The **M**-DOBDC MOFs demonstrate thus high reversibility to (i) release/absorb the two

DMF molecules; and (ii) be deprotonated (lithiated) / protonated (delithiated) reversibly. Chemical and structural stability is considered essential for MOFs application, positioning thus Li_2/H_2-**M**-DOBDC frameworks as promising structures, in contrast to other reported MOFs that experience irreversible phase transformation or structure collapse under similar processing conditions.[47] Considering the evidence provided, it is reasonable to deduce that Mn/Mg(II) metal nodes are exclusively coordinated through carboxylates and not phenolate functions. Important are the differences with respect to the phase reported by Jouhara *et al*.[36] Despite different chemical composition (Mn *vs* Mg), the PXRD pattern of Li_2-**Mn**-DOBDC is found to be utterly similar to that of Mg(Li_2)-*p*-DHT phase. Differences are noted in the relative intensity of certain peaks and the presence of a π-π stacking diffraction peak at 2θ = 30° only in the Mg(Li_2)-*p*-DHT phase (Figures 2A and S6). In contrast, although Li_2-**Mg**-DOBDC is of same composition as Mg(Li_2)-*p*-DHT, different phases are obtained (Figures 2A and S6). The electrochemistry of these is discussed in the following.

2.2. Electroactivity in Li_2-M-DOBDC MOFs: more than a sum of parts.

A prerequisite for electrical conductivity in MOFs is the efficient charge transport enabled either by an extended conjugation or by through-space interaction within organic moieties (*e.g.*, π-π stacking).[19,48] Dincă and co-workers developed analogs of the CPO-27 MOFs wherein replacing the oxygen by sulfur atom resulted in considerable enhancement of the electrical conductivity.[49,50,51] Herein, we probe the SBU and cation exchange impact on charge transport properties. Variable-temperature conductivity measurements were conducted on pressed-pellets using two-probe d.c. current−voltage technique (Figure 3a and Table 1, refer to SI and Figure S7 for details). All samples show semiconducting behavior with activation energy in the range of reported values for similar compositions, with however also significant differences. The Li_x-**Mn**-DOBDC MOFs (x=2, 1.5, 1) have considerably lower activation energy (E_a= 0.37 eV) than Li_2-**Mg**-DOBDC (E_a = 0.67 eV), H_2-**Mn**-DOBDC (E_a = 0.60 eV) or Mn-CPO-27 (E_a = 0.55 eV),[49] suggesting smaller band gap and hence higher charge carrier density in Li_x-**Mn**-DOBDC.

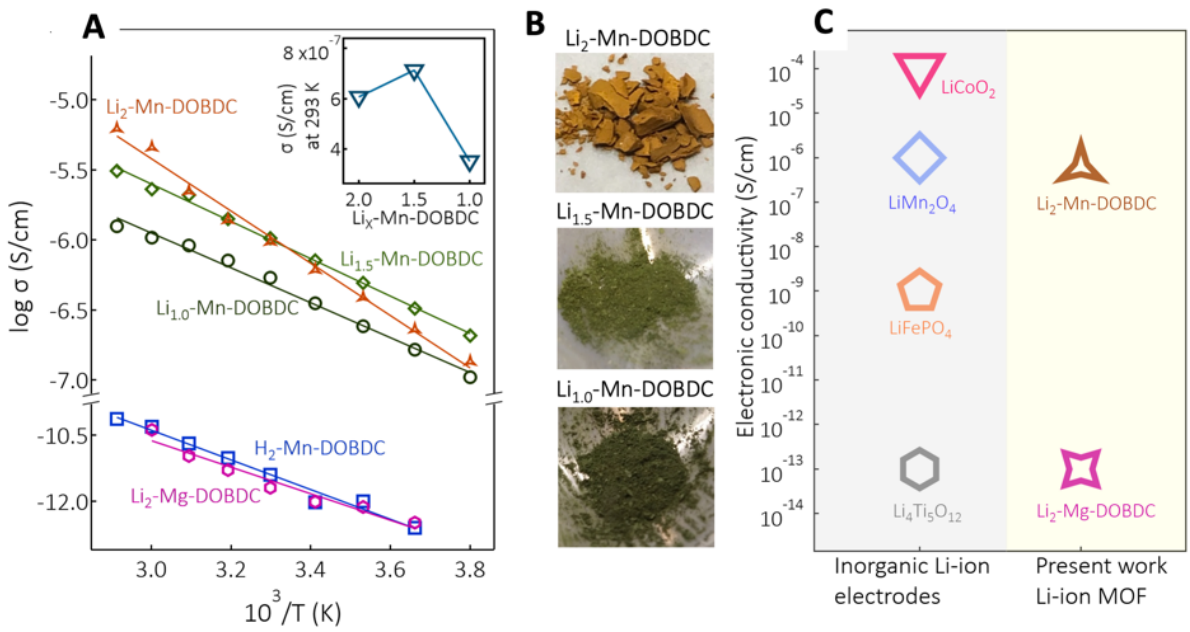

*Figure 3. (A) Variable temperature electronic conductivity plots for Li_x/H_2-**M**-DOBDC (**M** = Mn, Mg). The inset shows the conductivity at 293 K for Li_x-**Mn**-DOBDC phases with different lithium content (or corresponding oxidation extent, x=2, 1.5, 1). (B) Photographs of Li_x-**Mn**-DOBDC powders prepared by controlled chemical oxidation. (C) Electronic conductivity comparison of commercial inorganic LIB electrodes and of Li_2-**M**-DOBDC (M= Mn, Mg) phases.*

Table 1. Electronic conductivity of Li_2/H_2-M-DOBDC (M = Mn, Mg) and Mn-CPO-27.

	σ (S/cm)[a]	E_a (eV)[b]
Li_2-**Mn**-DOBDC	6.1×10^{-7}	0.37
Li_2-**Mg**-DOBDC	4.9×10^{-13}	0.67
H_2-**Mn**-DOBDC	7.4×10^{-13}	0.60
Mn-CPO-27[c]	3.0×10^{-13}	0.55
$Li_{1.5}$-**Mn**-DOBDC	7.1×10^{-7}	0.26
$Li_{1.0}$-**Mn**-DOBDC	3.5×10^{-7}	0.25

[a]Electrical conductivity at 293 K, [b]Activation energy, [c]Electrical conductivity at 297 K and Activation energy values of Mn-CPO-27 are taken from literature[49]

Notably, the difference in electronic structure of the redox-innocent $3s^0$ Mg^{2+} and the redox-active $3d^5$ Mn^{2+} is found responsible for the enhanced conductivity, indicating that not only the topology, but also the electronic structure of the metal ions plays important role in charge conduction. The conductivity of Li_2-**Mn**-DOBDC is six orders of magnitude higher than of the protonated H_2-**Mn**-

DOBDC or Mn_2-DOBDC (Mn-CPO-27)[49] analogues (Table 1). The most accountable reasons for hindering the charge transfer are the redox innocence of the phenolate-groups in the protonated H_2-$DOBDC^{2-}$ linker (in H_2-**Mn**-DOBDC) or binding to the transition metal node (in Mn-CPO-27); whereas the redox inactive nature of Mg^{2+} accounts for the low conductivity measured in Li_2-**Mg**-DOBDC. The presence of donor and acceptor components in the Li_2-**Mn**-DOBDC, promoting the charge-transfer interactions, with additional redox-matching and mixed valence ultimately explains the high electronic conductivity of only this phase.

We also synthesized and isolated the half-electron $Li_{1.5}$-**Mn**-DOBDC and one-electron oxidized $Li_{1.0}$-**Mn**-DOBDC forms (Figure 3b and S8) and evaluated their electronic conductivity. Within the measurement accuracy and experimental errors, the $Li_{1.5}$-**Mn**-DOBDC phase reaches a higher conductivity ($\sigma = 7.1 \times 10^{-7}$ S/cm) whereas further oxidation leads to insignificant decrease in $Li_{1.0}$-**Mn**-DOBDC ($\sigma = 3.5 \times 10^{-7}$ S/cm, Figure 3a inset, Table 1). In the case of $Li_{1.5}$-**Mn**-DOBDC, the charge mobility could likely be enhanced by facile hopping mechanism arising from radical anion/mixed valency.[52,7,50,51] Whereas, in the case of $Li_{1.0}$-**Mn**-DOBDC, the hopping charge mobility could be disturbed by the presence of semi-quinone radical on the phenyl ring. The conductivity of the Li_x-**Mn**-DOBDC phases is the highest attained with this stereotypical DOBDC ligand and it is comparable to best conducting M_2(DEBDC) (M = Fe, Mn; E = S, O) frameworks.[49] These results are highly encouraging with respect to organic electrode materials, wherein electronic conductivities are in the range of $\sigma = 10^{-10}$-10^{-15} S/cm,[53,54] and thereby putting forward MOFs as efficient strategy towards conductive organic-based electrode materials without any compromise in energy metrics. The conductivity is also on par to that of inorganic Li-ion materials with the conductivity similar to $LiMn_2O_4$, and surpassing that of $LiFePO_4$ and $Li_4Ti_5O_{12}$ (Figure 3C).

2.3. Electrochemistry of $DOBDC^{4-}$ based MOFs–the penalty of synergy.

The solid-state electrochemistry of the Li_2-**Mn**-DOBDC phase was evaluated in Li half-cells, along with Li_2-**Mg**-DOBDC and Mn-CPO-27 in order to correlate the electroactivity with the composition, topology, and physico-chemical features discussed above. The electrochemical performances were first investigated as a function of charge (oxidation) cut-off potential until irreversible redox processes were noticed (Figure 4). As with Fe_2-DOBDC,[32] Mn-CPO-27 (Mn_2-DOBDC) was also found to display irreversible redox regardless of electrode composition and cycling conditions (Figure 4A). During the charge (oxidation) process, Mn-CPO-27 shows a short - sloping, followed by a long - flat plateau, accounting for more than one electron oxidation. In contrast, on discharge, the electrode shows a total loss of electrochemical activity, with only a minor electrochemical response detected at 3.25V vs. Li^+/Li (marked with R1, Figure 4A) and 2.4V vs. Li^+/Li (marked with R2, Figure 4A).

Note that the charge cut-off voltage has an influence on the presence of R1 and R2 responses (Figure S9). The R2 response matches the typical redox potential value of Li_4-DOBDC (defined in literature also as Li_4-*p*-DHT or $Li_4C_8H_2O_6$),[36,40] whereas the R1 signature is of a more complex nature. We believe that the Mn^{2+}/Mn^{3+} redox couple is activated in Mn-CPO-27 at high potentials (> 3.8V) leading to Mn^{3+} disproportionation (Scheme 2A), followed by MOF structure decomposition, with traces of oxidized Li_{2-x}-**Mn**-DOBDC (R1) and Li_{4-x}-DOBDC (R2) phases obtained.[55,56] Whereas additional analyses may be required to better apprehend the precise degradation mechanism and reactivity pathways, the irreversible redox in Mn-CPO-27 remains congruent with Aubrey's results and could be further generalized to other CPO-27 compositions with different metal centres.

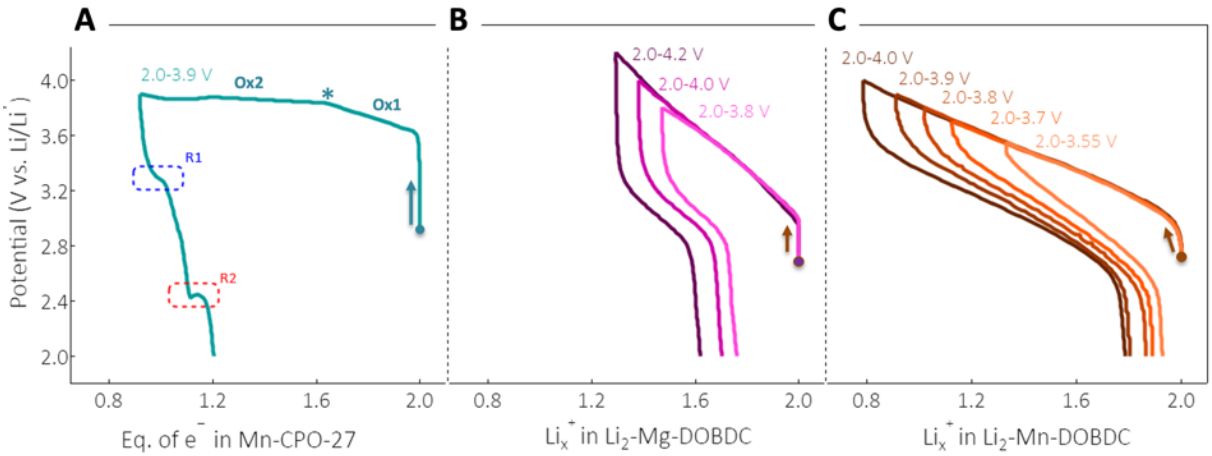

*Figure 4. Potential – composition profiles of Mn-CPO-27 (A), Li_2-**Mg**-DOBDC (B) and Li_2-**Mn**-DOBDC (C) electrodes measured in Li half-cell configuration. All cells were started in charge (oxidation) mode (marked by dot and arrow). The galvanostatic reaction rate applied for all tests is of 1 electron exchanged in 10 hours per unit formula. Red and blue dashed squares (R1/R2) corresponding to typical redox of DOBDC ligand partially bound to Mn (R1, Li_{2-x}-**Mn**-DOBDC) or of Li_{4-x}-DOBDC phase (R2).*

Conversely, better reversibility and higher stability is found for Li_2-**Mg**-DOBDC and Li_2-**Mn**-DOBDC (Figures 4B, 4C). Except similar slopped voltage profiles, characteristic of a solid solution process,[57,58,59] both compositions display noticeable differences in terms of reversibility, electrode polarization and attained material utilisation within a specific redox potential window (Figures 4B,C). For a given potential cycling window of 2.0-4.0 V, reversible exchange of 0.3 and 1.1 e^-/Li^+ equivalents was possible to attain for Li_2-**Mg**-DOBDC and Li_2-**Mn**-DOBDC, respectively. The charge cut-off potential has also an impact on the reversible specific capacities attained (Figures 4B, 4C, S9). A noticeable fact is the appearance of R2 response for Li_2-**Mn**-DOBDC when more than 1.3 e^-/Li^+ equivalents is extracted

(Figure S9), implying partial degradation, and raising questions on the nature of the redox mechanism for these MOF systems.

When cycled at the same current density, Li_2-**Mg**-DOBDC displays higher polarization as compared to the Li_2-**Mn**-DOBDC phase, which can be explained by orders of magnitude lower electronic conductivity. Curiously, the same does not apply to the similar composition but different phase (Mg)Li_2-*p*-DHT reported by Jouhara *et al.*,[36] where a much lower polarization was measured. This could be accounted for structural differences between the two Mg phases, notably the presence of π-π stacking diffraction peak at 2θ = 30° (Figure2A), but also differences in ionic and electronic conductivities between both phases (further discussion is provided in Figure S9). According to the same work, the redox potential of $DOBDC^{4-}$ center can be significantly influenced by the polarizing power of the metal cation used. The reported metal cations were redox innocent (e.g., Li^+, Ba^{2+}, Ca^{2+} and Mg^{2+}) and were not expected to participate in the redox. Here, we employed a redox active transition metal (Mn^{2+}) which might participate to the overall redox reaction. Based on this, we are suggesting possible electrochemical reaction pathways highlighting the effect of Mn^{2+} mediated versus Mg^{2+} non-mediated redox as illustrated in Scheme 2.

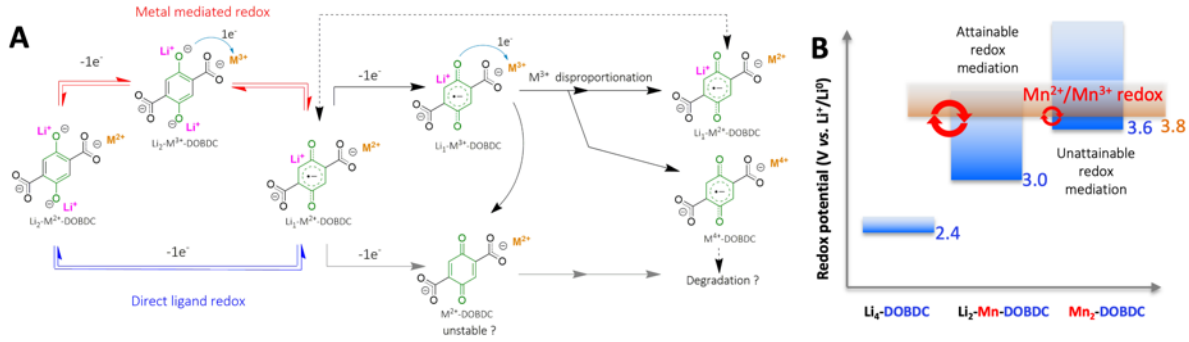

*Scheme 2. (A) Proposed scheme for redox redox pathways in Li_2-**M**-DOBDC (M= Mn and Mg) highlighting M^{2+} redox mediated vs. redox non-mediated. (B) Estimated redox potentials of DOBDC ligand (blue blocks) and of $Mn^{2+/3+}$ redox couples (orange block) for the studied Li_x-**Mn_y**-DOBDC phases (x=4, 2, 0 and y=0, 1, 2, respectively).*

Direct ligand centered oxidation in Li_2-**Mn^{2+}**-DOBDC (to yield Li_1-**Mn^{2+}**-DOBDC, blue path in Scheme 2A) is the most plausible reaction pathway here. Concurrently, and given the possible overlap between ligand and $Mn^{2+/3+}$ redox (Scheme 2B) the oxidation can also proceed through transient formation of Mn^{3+}-DOBDC (Li_1-**Mn^{3+}**-DOBDC) which mediates the oxidation of the ligand and leads to

the formation of the semi-quinone Li_1-**Mn^{2+}**-DOBDC thermodynamic product (red path in Scheme 2A). A similar redox pathway was also observed during chemical oxidation of Mn-CPO-27.[34] In contrast, the redox in Li_2-**Mg^{2+}**-DOBDC exclusively proceeds on the organic center (blue path in Scheme 2A). The irreversible process observed with Mn-CPO-27 (Figure 4A) might have a more complex origin, with Mn^{3+} species disproportionation[60,61] and MOF degradation (black path in Scheme 2A, supported by experiments analysis in Figure 4A). The incorporation of Mn^{2+} in Li_2-**Mn**-DOBDC induces a significant increase in redox potential by nearly 800 mV with respect to Li_4-DOBDC,[36,40,41,42,43] attributed to the high ionic potential and polarizing power of Mn^{2+}.[18,36,62] Upon second Mn^{2+} (or Mg^{2+}) incorporation, further redox potential increase is expected, and the $Mn^{2+/3+}$ mediation might not be possible (Scheme 2B, the case for Mn_2-DOBDC). This also corroborates the use of strong oxidizing agents applied for Fe-CPO-27 (Fe_2-DOBDC)[32] and Mn-CPO-27.[35] This is also observed in our experiments, wherein the charge cut-off was found as high as 3.65 V (Ox1, Figure 4A), followed by overlap with irreversible redox at 3.85 V (Ox2, Figure 4A and Scheme 2B). The former being attributed to $DOBDC^{4-/3-}$, whereas the latter to $Mn^{2+/3+}$ redox couple.

2.4 Lithium storage performance of Li_2-Mn-DOBDC electrodes.

We next analyse the charge storage performances. Considering the intrinsic electrical conductivity, lowest polarization and higher reversibility, we focused our study only on Li_2-**Mn**-DOBDC phase. First, various electrolyte compositions have been screened and compared for equivalent Li_2-**Mn**-DOBDC composition electrodes (Figure S10). For all formulations, whereas the supporting salt shows no significant effect, the electrolyte solvent impacts the Coulombic Efficiency (CE) and capacity retention. For instance, good capacity retention of 60-80% was obtained with ether-based solvents, as compared to only 40% with ionic liquids, when using LiTFSI salt. Similar feature was also observed with $LiPF_6$ in carbonate-based solvent. The best performance is attained with 1M LiTFSI in DOL/DME with a capacity retention of 91% and average CE of 99.7% after 100 cycles (Figure 5). Similarly to other DOBDC analogues,[63] Li_2-**Mg**-DOBDC and Li_2-**Mn**-DOBDC delivered lower capacities than expected (*e.g.*, redox process limited to <1 instead of 2 electrons theoretically). This was assigned to stabilizing effect of the semi-quinone radical anion due to inter-molecular π-π interactions, alike the p-type poly(vinylphenonthiazine) electrode material.[64] This assumption might be valid for (Mg)Li_2-*p*-DHT as it indeed reveals a π-π stacked structure, but is not applicable to Li_2-**Mg**-DOBDC and Li_2-**Mn**-DOBDC as both are free of any significant π-π interactions (Figures 2A and S6) with the true nature of intrinsic limitation of the redox in this particular ligand remaining an open question.

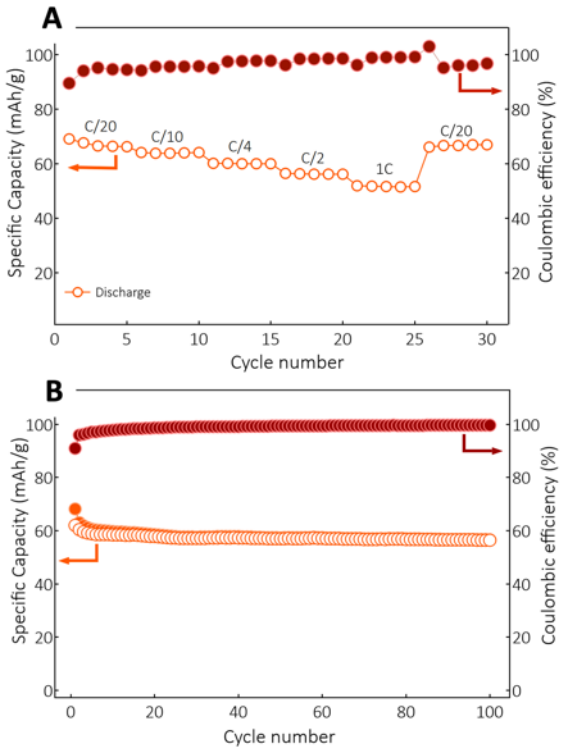

*Figure 5. Capacity – rate test (a) and capacity retention at a rate of 2C (b) in Li half-cells using Li_2-**Mn**-DOBDC as the active electrode and 1M LiTFSI in DOL/DME as the electrolyte.*

The Li^+ storage performance of Li_2-**Mn**-DOBDC was also evaluated for different conducting carbon loadings and cycling rates. Higher specific capacity was delivered by using 40 wt.% of carbon (Figure S11), while still attaining high capacities for lower carbon amounts. This limitation could stems from suboptimal electrode microstructure, bad adequacy of texture and contact between conductive carbon and Li_2-**Mn**-DOBDC particles.[65] The rate capability was investigated under different cycling rates ranging from C/20 to 1C (Figure 5a). Despite the non-optimized electrode architecture, the capacity delivered by Li_2-**Mn**-DOBDC does not appear to be affected even at high currents. In fact, the capacity is marginally decreased as the cycling rate increased up to 1C, for which 83% of the capacity coupled with good coulombic efficiency and low polarization are maintained (Figure S12). When going back to C/20, the initial capacity is recovered indicating that the losses are due to kinetic limitations of the electrode and not structural or chemical degradation. The intrinsic electronic conductivity of different redox intermediates (*e.g.* Li_x-**Mn**-DOBDC; x = 1, 1.5, 2; Figure 3) is beneficial for stable charge and discharge process under at high rates (Figures 5a and S12). Finally, thanks to the rigid inter-connected framework, Li_2-**Mn**-DOBDC demonstrates an excellent cycling stability by maintaining 91% of its capacity accompanied with high coulombic efficiency (99.7%) over 100 cycles (Figure 5b).

CONCLUSION

A series of electrically conducting Li-ion MOFs with general formula Li_x-**M**-DOBDC (where x= 1, 1.5, 2; **M** = Mg^{2+} or Mn^{2+}; $DOBDC^{4-}$ = 2,5-dihydroxybenzene-1,4-dicarboxylate) are prepared and studied for the first time. The rational control of the ligand-metal coordination modes and SBU topology in the archetypical MOF-74 allowed post-synthetic lithiation of the uncoordinated phenolic redox sites. The lithiation process is reversible implying high framework robustness during metalation which provides additional perspectives for trans-metalation (*e.g.* other alkali or transition metal cations) of conducting MOFs. This judicious chemical and structural transformation enable superior metal-ligand interaction in the framework inducing a million-fold increase in electrical conductivity facilitated by mix-in redox: 10^{-7} S/cm for Li_2-**Mn**-DOBDC *vs.* 10^{-13} S/cm for the isoreticular H_2-**Mn**-DOBDC and Li_2-**Mg**-DOBDC. As redox active material, Li_2-**Mn**-DOBDC demonstrates promising electrochemical performances: *e.g.* 91% capacity retention over 100 cycles at a high average discharge potential of 3.2V vs. Li^+/Li^0. Whereas the specific capacities obtained with these MOF cathodes remain lower than expected, it is supposedly penalized by the intrinsic limitations of the DOBDC linker. The innovative design strategy suggested in this work could be applied to other linkers and transition metal chemistries to increase the specific capacity, output voltage, and thus achieving higher energy densities for application of MOFs in next generation rechargeable batteries. This work opens up frontiers in development of electrically conducting MOFs for electrochemical energy storage applications by introducing the new class of Li-cation reservoir MOF materials with reversible redox.

ASSOCIATED CONTENT

Supporting Online information includes Sections detailing on Materials and Methods; Extended literature review of SBU topologies for DOBDC based MOFs; Extended literature review of MOF cathode materials; Crystal structure details; as well as Additional Data, Figures and Discussion.

CORRESPONDING AUTHOR

alexandru.vlad@uclouvain.be

ACKNOWLEDGMENTS

A.V. is indebted to the European Research Council under the European Union's Horizon 2020 research and innovation program (grant agreement no. 770870, MOOiRE, ERC-CoG). The authors declare no

competing financial interests. We thank Prof. Philippe POIZOT for providing the raw PXRD and FTIR data for (Mg)Li_2-*p*-DHT phase, as well as for insightful discussions.

REFERENCES

(1) Armand, M.; Tarascon, J. M. Building Better Batteries. *Nature* **2008**, *451* (7179), 652–657. https://doi.org/10.1038/451652a.

(2) Larcher, D.; Tarascon, J. M. Towards Greener and More Sustainable Batteries for Electrical Energy Storage. *Nat. Chem.* **2015**, *7* (1), 19–29. https://doi.org/10.1038/nchem.2085.

(3) Poizot, P.; Gaubicher, J.; Renault, S.; Dubois, L.; Liang, Y.; Yao, Y. Opportunities and Challenges for Organic Electrodes in Electrochemical Energy Storage. *Chemical Reviews*. July 22, 2020, pp 6490–6557. https://doi.org/10.1021/acs.chemrev.9b00482.

(4) Poizot, P.; Dolhem, F. Clean Energy New Deal for a Sustainable World: From Non-CO2 Generating Energy Sources to Greener Electrochemical Storage Devices. *Energy Environ. Sci.* **2011**, *4* (6), 2003–2019. https://doi.org/10.1039/c0ee00731e.

(5) Esser, B.; Dolhem, F.; Becuwe, M.; Poizot, P.; Vlad, A.; Brandell, D. A Perspective on Organic Electrode Materials and Technologies for next Generation Batteries. *J. Power Sources* **2021**, *482* (July 2020), 228814. https://doi.org/10.1016/j.jpowsour.2020.228814.

(6) Zhang, Z.; Awaga, K. Redox-Active Metal-Organic Frameworks as Electrode Materials for Batteries. *MRS Bull.* **2016**, *41* (11), 883–889. https://doi.org/10.1557/mrs.2016.245.

(7) D'Alessandro, D. M. Exploiting Redox Activity in Metal-Organic Frameworks: Concepts, Trends and Perspectives. *Chem. Commun.* **2016**, *52* (58), 8957–8971. https://doi.org/10.1039/c6cc00805d.

(8) Zhao, R.; Liang, Z.; Zou, R.; Xu, Q. Metal-Organic Frameworks for Batteries. *Joule* **2018**, *2* (11), 2235–2259. https://doi.org/10.1016/j.joule.2018.09.019.

(9) Wang, H.; Zhu, Q. L.; Zou, R.; Xu, Q. Metal-Organic Frameworks for Energy Applications. *Chem* **2017**, *2* (1), 52–80. https://doi.org/10.1016/j.chempr.2016.12.002.

(10) Shrivastav, V.; Sundriyal, S.; Goel, P.; Kaur, H.; Tuteja, S. K.; Vikrant, K.; Kim, K. H.; Tiwari, U. K.; Deep, A. Metal-Organic Frameworks (MOFs) and Their Composites as Electrodes for Lithium Battery Applications: Novel Means for Alternative Energy Storage. *Coord. Chem. Rev.* **2019**, *393*, 48–78. https://doi.org/10.1016/j.ccr.2019.05.006.

(11) Wang, Z.; Tao, H.; Yue, Y. Metal-Organic-Framework-Based Cathodes for Enhancing the Electrochemical Performances of Batteries: A Review. *ChemElectroChem* **2019**, *6* (21), 5358–5374. https://doi.org/10.1002/celc.201900843.

(12) Zhang, Y.; Riduan, S. N.; Wang, J. Redox Active Metal- and Covalent Organic Frameworks for Energy Storage: Balancing Porosity and Electrical Conductivity. *Chem. - A Eur. J.* **2017**, *23* (65), 16419–16431. https://doi.org/10.1002/chem.201702919.

(13) Sheberla, D.; Bachman, J. C.; Elias, J. S.; Sun, C. J.; Shao-Horn, Y.; Dincă, M. Conductive MOF Electrodes for Stable Supercapacitors with High Areal Capacitance. *Nat. Mater.* **2017**, *16* (2), 220–224. https://doi.org/10.1038/nmat4766.

(14) Xiao, P.; Bu, F.; Zhao, R.; Aly Aboud, M. F.; Shakir, I.; Xu, Y. Sub-5 Nm Ultrasmall Metal−Organic Framework Nanocrystals for Highly Efficient Electrochemical Energy Storage Article. *ACS Nano* **2018**, *12*, 58. https://doi.org/10.1021/acsnano.8b01488.

(15) Xiao, P.; Li, S.; Yu, C.; Wang, Y.; Xu, Y. Interface Engineering between the Metal− Organic Framework Nanocrystal and Graphene toward Ultrahigh Potassium-Ion Storage Performance. *ACS Nano* **2020**, *14*, 10210–10218. https://doi.org/10.1021/acsnano.0c03488.

(16) Fan, M.; Liao, D.; Aboud, M. F. A.; Shakir, I.; Xu, Y. A Universal Strategy toward Ultrasmall Hollow Nanostructures with Remarkable Electrochemical Performance. *Angew. Chemie* **2020**, *132* (21), 8324–8331. https://doi.org/10.1002/ange.202000352.

(17) Wang, K.; Hui, K. N.; San Hui, K.; Peng, S.; Xu, Y. Recent Progress in Metal-Organic Framework/Graphene-Derived Materials for Energy Storage and Conversion: Design, Preparation, and Application. *Chemical Science*. 2021, pp 5737–5766. https://doi.org/10.1039/d1sc00095k.

(18) Lakraychi, A. E.; De Kreijger, S.; Gupta, D.; Elias, B.; Vlad, A. Phendione–Transition-Metal Complexes with Bipolar Redox Activity for Lithium Batteries. *ChemSusChem* **2020**, *13* (9), 2225–2231. https://doi.org/10.1002/cssc.201903290.

(19) Xie, L. S.; Skorupskii, G.; Dincă, M. Electrically Conductive Metal–Organic Frameworks. *Chem. Rev.* **2020**, *120* (16), 8536–8580. https://doi.org/10.1021/acs.chemrev.9b00766.

(20) Wang, D.-Y.; Liu, R.; Guo, W.; Li, G.; Fu, Y. Recent Advances of Organometallic Complexes for Rechargeable Batteries. *Coord. Chem. Rev.* **2020**, 213650. https://doi.org/https://doi.org/10.1016/j.ccr.2020.213650.

(21) Férey, G.; Millange, F.; Morcrette, M.; Serre, C.; Doublet, M.-L.; Grenèche, J.-M.; Tarascon, J.-M. Mixed-Valence Li/Fe-Based Metal–Organic Frameworks with Both Reversible Redox and Sorption Properties. *Angew. Chemie Int. Ed.* **2007**, *46* (18), 3259–3263. https://doi.org/10.1002/anie.200605163.

(22) de Combarieu, G.; Morcrette, M.; Millange, F.; Guillou, N.; Cabana, J.; Grey, C. P.; Margiolaki, I.; Férey, G.; Tarascon, J.-M. Influence of the Benzoquinone Sorption on the Structure and Electrochemical Performance of the MIL-53(Fe) Hybrid Porous Material in a Lithium-Ion Battery. *Chem. Mater.* **2009**, *21* (8), 1602–1611. https://doi.org/10.1021/cm8032324.

(23) Fateeva, A.; Horcajada, P.; Devic, T.; Serre, C.; Marrot, J.; Grenèche, J.; Morcrette, M.; Tarascon, J.; Maurin, G.; Férey, G. Synthesis , Structure , Characterization , and Redox Properties of the Porous MIL-68 (Fe) Solid. **2010**, *68*, 3789–3794. https://doi.org/10.1002/ejic.201000486.

(24) Gu, S.; Bai, Z.; Majumder, S.; Huang, B.; Chen, G. Conductive Metal–Organic Framework with Redox Metal Center as Cathode for High Rate Performance Lithium Ion Battery. *J. Power Sources* **2019**, *429* (May), 22–29. https://doi.org/10.1016/j.jpowsour.2019.04.087.

(25) Dühnen, S.; Nölle, R.; Wrogemann, J.; Winter, M.; Placke, T. Reversible Anion Storage in a Metal-Organic Framework for Dual-Ion Battery Systems. *J. Electrochem. Soc.* **2019**, *166* (3), A5474–A5482. https://doi.org/10.1149/2.0681903jes.

(26) Tian, B.; Ning, G.-H.; Gao, Q.; Tan, L.-M.; Tang, W.; Chen, Z.; Su, C.; Loh, K. P. Crystal Engineering of Naphthalenediimide-Based Metal–Organic Frameworks: Structure-Dependent Lithium Storage. *ACS Appl. Mater. Interfaces* **2016**, *8* (45), 31067–31075. https://doi.org/10.1021/acsami.6b11772.

(27) Zhang, Z.; Yoshikawa, H.; Awaga, K. Monitoring the Solid-State Electrochemistry of Cu(2,7-AQDC) (AQDC = Anthraquinone Dicarboxylate) in a Lithium Battery: Coexistence of Metal and Ligand Redox Activities in a Metal–Organic Framework. *J. Am. Chem. Soc.* **2014**, *136* (46), 16112–16115. https://doi.org/10.1021/ja508197w.

(28) Zhang, Z.; Yoshikawa, H.; Awaga, K. Discovery of a "Bipolar Charging" Mechanism in the Solid-State Electrochemical Process of a Flexible Metal–Organic Framework. *Chem. Mater.* **2016**, *28* (5), 1298–1303. https://doi.org/10.1021/acs.chemmater.5b04075.

(29) Ziebel, M. E.; Gaggioli, C. A.; Turkiewicz, A. B.; Ryu, W.; Gagliardi, L.; Long, J. R. Effects of Covalency on Anionic Redox Chemistry in Semiquinoid-Based Metal–Organic Frameworks. *J. Am. Chem. Soc.* **2020**, *142* (5), 2653–2664. https://doi.org/10.1021/jacs.9b13050.

(30) Jiang, Q.; Xiong, P.; Liu, J.; Xie, Z.; Wang, Q.; Yang, X.; Hu, E.; Cao, Y.; Sun, J.; Xu, Y.; Chen, L. A Redox-Active 2D Metal–Organic Framework for Efficient Lithium Storage with Extraordinary High Capacity. *Angew. Chemie* **2020**, 1–6. https://doi.org/10.1002/ange.201914395.

(31) Lou, X.; Geng, F.; Hu, B.; Li, C.; Shen, M.; Hu, B. Reversible High-Voltage N-Redox Chemistry in Metal-Organic Frameworks for High-Rate Anion-Intercalation Batteries. *ACS Appl. Energy Mater.* **2019**, *2* (1), 413–419. https://doi.org/10.1021/acsaem.8b01428.

(32) Aubrey, M. L.; Long, J. R. A Dual-Ion Battery Cathode via Oxidative Insertion of Anions in a Metal-Organic Framework. *J. Am. Chem. Soc.* **2015**, *137* (42), 13594–13602. https://doi.org/10.1021/jacs.5b08022.

(33) Peng, Z.; Yi, X.; Liu, Z.; Shang, J.; Wang, D. Triphenylamine-Based Metal–Organic Frameworks as Cathode Materials in Lithium-Ion Batteries with Coexistence of Redox Active Sites, High Working Voltage, and High Rate Stability. *ACS Appl. Mater. Interfaces* **2016**, *8* (23), 14578–14585. https://doi.org/10.1021/acsami.6b03418.

(34) Park, S. S.; Tulchinsky, Y.; Dinca, M. Single-Ion Li+, Na+, and Mg2+ Solid Electrolytes Supported by a Mesoporous Anionic Cu-Azolate Metal-Organic Framework. *J. Am. Chem. Soc.* **2017**, *139* (38), 13260–13263. https://doi.org/10.1021/jacs.7b06197.

(35) Cozzolino, A. F.; Brozek, C. K.; Palmer, R. D.; Yano, J.; Li, M.; Dincă, M. Ligand Redox Non-Innocence in the Stoichiometric Oxidation of Mn 2 (2,5-Dioxidoterephthalate) (Mn-MOF-74). *J. Am. Chem. Soc.* **2014**, *136* (9), 3334–3337. https://doi.org/10.1021/ja411808r.

(36) Jouhara, A.; Dupré, N.; Gaillot, A. C.; Guyomard, D.; Dolhem, F.; Poizot, P. Raising the Redox Potential in Carboxyphenolate-Based Positive Organic Materials via Cation Substitution. *Nat. Commun.* **2018**, *9* (1). https://doi.org/10.1038/s41467-018-06708-x.

(37) Poizot, P.; Cadiou, V.; Gaillot, A.-C.; Deunf, E.; Dolhem, F.; Dubois, L.; Gutel, T. Pairing Cross-Linked Polyviologen with Aromatic Amine Host Structure for Anion Shuttle Rechargeable Batteries. *ChemSusChem* **2020**. https://doi.org/10.1002/cssc.201903578.

(38) Harris, D. *Function of Quinones in Energy Conserving Systems*; Trumpower, B. L., Ed.; Elsevier, 1982; Vol. 13. https://doi.org/10.1016/B978-0-12-701280-3.X5001-4.

(39) Peover, M. E. 879. A Polarographic Investigation into the Redox Behaviour of Quinones: The Roles of Electron Affinity and Solvent. *J. Chem. Soc.* **1962**, 4540. https://doi.org/10.1039/jr9620004540.

(40) Renault, S.; Gottis, S.; Barrès, A. L.; Courty, M.; Chauvet, O.; Dolhem, F.; Poizot, P. A Green Li-Organic Battery Working as a Fuel Cell in Case of Emergency. *Energy Environ. Sci.* **2013**, *6* (7), 2124–2133. https://doi.org/10.1039/c3ee40878g.

(41) Quarez, É.; Jouhara, A.; Grolleau, S.; Dolhem, F.; Dupré, N.; Poizot, P. From Partial to Complete Neutralization of 2,5-Dihydroxyterephthalic Acid in the Li–Na System: Crystal Chemistry and Electrochemical Behavior of Na 2 Li 2 C 8 H 2 O 6 vs. Li . *CrystEngComm* **2020**. https://doi.org/10.1039/c9ce01674k.

(42) Wang, S.; Wang, L.; Zhang, K.; Zhu, Z.; Tao, Z.; Chen, J. Organic Li4C8H2O6 Nanosheets for Lithium-Ion Batteries. *Nano Lett.* **2013**, *13* (9), 4404–4409. https://doi.org/10.1021/nl402239p.

(43) Zhao, Q.; Wang, J.; Chen, C.; Ma, T.; Chen, J. Nanostructured Organic Electrode Materials Grown on Graphene with Covalent-Bond Interaction for High-Rate and Ultra-Long-Life Lithium-Ion Batteries. *Nano Res.* **2017**, *10* (12), 4245–4255. https://doi.org/10.1007/s12274-017-1580-9.

(44) Jayaramulu, K.; Kanoo, P.; George, S. J.; Maji, T. K. Tunable Emission from a Porous Metal-Organic Framework by Employing an Excited-State Intramolecular Proton Transfer Responsive Ligand. *Chem. Commun.* **2010**, *46* (42), 7906–7908. https://doi.org/10.1039/c0cc02069a.

(45) Shustova, N. B.; Cozzolino, A. F.; Reineke, S.; Baldo, M.; Dincă, M. Selective Turn-on Ammonia Sensing Enabled by High-Temperature Fluorescence in Metal-Organic Frameworks with Open Metal Sites. *J. Am. Chem. Soc.* **2013**, *135* (36), 13326–13329. https://doi.org/10.1021/ja407778a.

(46) Chaemchuem, S.; Kui, Z.; Verpoort, F. Control of Interpenetration via in Situ Lithium Incorporation in MOFs and Their Gas Adsorption Properties and Selectivity. *CrystEngComm* **2016**, *18* (39), 7614–7619. https://doi.org/10.1039/C6CE01522K.

(47) Howarth, A. J.; Liu, Y.; Li, P.; Li, Z.; Wang, T. C.; Hupp, J. T.; Farha, O. K. Chemical, Thermal and Mechanical Stabilities of Metal-Organic Frameworks. *Nat. Rev. Mater.* **2016**, *1* (15018), 1–15. https://doi.org/10.1038/natrevmats.2015.18.

(48) Xie, L. S.; Alexandrov, E. V.; Skorupskii, G.; Proserpio, D. M.; Dincă, M. Diverse π-π Stacking Motifs Modulate Electrical Conductivity in Tetrathiafulvalene-Based Metal-Organic Frameworks. *Chem. Sci.* **2019**, *10* (37), 8558–8565. https://doi.org/10.1039/c9sc03348c.

(49) Sun, L.; Hendon, C. H.; Minier, M. A.; Walsh, A.; Dincă, M. Million-Fold Electrical Conductivity Enhancement in Fe 2 (DEBDC) versus Mn 2 (DEBDC) (E = S, O). *J. Am. Chem. Soc.* **2015**, *137* (19), 6164–6167. https://doi.org/10.1021/jacs.5b02897.

(50) Walsh, A.; Butler, K. T.; Hendon, C. H. Chemical Principles for Electroactive Metal-Organic Frameworks. *MRS Bull.* **2016**, *41* (11), 870–876. https://doi.org/10.1557/mrs.2016.243.

(51) Sun, L.; Campbell, M. G.; Dincə, M. Electrically Conductive Porous Metal-Organic Frameworks. *Angew. Chemie - Int. Ed.* **2016**, *55* (11), 3566–3579. https://doi.org/10.1002/anie.201506219.

(52) Calbo, J.; Golomb, M. J.; Walsh, A. Redox-Active Metal-Organic Frameworks for Energy Conversion and Storage. *J. Mater.*

Chem. A **2019**, *7* (28), 16571–16597. https://doi.org/10.1039/c9ta04680a.

(53) Lu, Y.; Chen, J. Prospects of Organic Electrode Materials for Practical Lithium Batteries. *Nat. Rev. Chem.* **2020**. https://doi.org/10.1038/s41570-020-0160-9.

(54) Dong, H.; Tutusaus, O.; Liang, Y.; Zhang, Y.; Lebens-Higgins, Z.; Yang, W.; Mohtadi, R.; Yao, Y. High-Power Mg Batteries Enabled by Heterogeneous Enolization Redox Chemistry and Weakly Coordinating Electrolytes. *Nat. Energy* **2020**, *5* (12), 1043–1050. https://doi.org/10.1038/s41560-020-00734-0.

(55) Zhou, G.; Sun, X.; Li, Q. H.; Wang, X.; Zhang, J. N.; Yang, W.; Yu, X.; Xiao, R.; Li, H. Mn Ion Dissolution Mechanism for Lithium-Ion Battery with LiMn2O4 Cathode: In Situ Ultraviolet-Visible Spectroscopy and Ab Initio Molecular Dynamics Simulations. *J. Phys. Chem. Lett.* **2020**, *11* (8), 3051–3057. https://doi.org/10.1021/acs.jpclett.0c00936.

(56) Zhan, C.; Wu, T.; Lu, J.; Amine, K. Dissolution, Migration, and Deposition of Transition Metal Ions in Li-Ion Batteries Exemplified by Mn-Based Cathodes-A Critical Review. *Energy Environ. Sci.* **2018**, *11* (2), 243–257. https://doi.org/10.1039/c7ee03122j.

(57) B. C. H. Steele in Superionic Conductors; G. D. Mahan, W. L. R., Ed.; Springer, Heidelberg, 1976; pp 47–64.

(58) Rozier, P.; Morcrette, M.; Martin, P.; Laffont, L.; Tarascon, J.-M. Solid Solution (Li1.3-YCuy)V3O8: Structure and Electrochemistry. *Chem. Mater.* **2005**, *17* (5), 984–991. https://doi.org/10.1021/cm048518f.

(59) Zhang, H.; Li, C.; Eshetu, G. G.; Laruelle, S.; Grugeon, S.; Zaghib, K.; Julien, C.; Mauger, A.; Guyomard, D.; Rojo, T.; Gisbert-Trejo, N.; Passerini, S.; Huang, X.; Zhou, Z.; Johansson, P.; Forsyth, M. From Solid-Solution Electrodes and the Rocking-Chair Concept to Today's Batteries. *Angew. Chemie - Int. Ed.* **2020**. https://doi.org/10.1002/anie.201913923.

(60) Liu, T.; Dai, A.; Lu, J.; Yuan, Y.; Xiao, Y.; Yu, L.; Li, M.; Gim, J.; Ma, L.; Liu, J.; Zhan, C.; Li, L.; Zheng, J.; Ren, Y.; Wu, T.; Shahbazian-Yassar, R.; Wen, J.; Pan, F.; Amine, K. Correlation between Manganese Dissolution and Dynamic Phase Stability in Spinel-Based Lithium-Ion Battery. *Nat. Commun.* **2019**, *10* (1), 4721. https://doi.org/10.1038/s41467-019-12626-3.

(61) Zhan, C.; Lu, J.; Jeremy Kropf, A.; Wu, T.; Jansen, A. N.; Sun, Y. K.; Qiu, X.; Amine, K. Mn(II) Deposition on Anodes and Its Effects on Capacity Fade in Spinel Lithium Manganate-Carbon Systems. *Nat. Commun.* **2013**, *4* (Ii), 1–8. https://doi.org/10.1038/ncomms3437.

(62) Sieuw, L.; Lakraychi, A. E.; Rambabu, D.; Robeyns, K.; Jouhara, A.; Borodi, G.; Morari, C.; Poizot, P.; Vlad, A. Through-Space Charge Modulation Overriding Substituent Effect: Rise of the Redox Potential at 3.35 V in a Lithium-Phenolate Stereoelectronic Isomer. *Chem. Mater.* **2020**, *32* (23), 9996–10006. https://doi.org/10.1021/acs.chemmater.0c02989.

(63) Gottis, S.; Barres, A. L.; Dolhem, F.; Poizot, P. Voltage Gain in Lithiated Enolate-Based Organic Cathode Materials by Isomeric Effect. *ACS Appl. Mater. Interfaces* **2014**, *6* (14), 10870–10876. https://doi.org/10.1021/am405470p.

(64) Kolek, M.; Otteny, F.; Schmidt, P.; Mück-Lichtenfeld, C.; Einholz, C.; Becking, J.; Schleicher, E.; Winter, M.; Bieker, P.; Esser, B. Ultra-High Cycling Stability of Poly(Vinylphenothiazine) as a Battery Cathode Material Resulting from π-π Interactions. *Energy Environ. Sci.* **2017**, *10* (11), 2334–2341. https://doi.org/10.1039/c7ee01473b.

(65) Lakraychi, A. E.; Dolhem, F.; Djedaïni-Pilard, F.; Thiam, A.; Frayret, C.; Becuwe, M. Decreasing Redox Voltage of Terephthalate-Based Electrode Material for Li-Ion Battery Using Substituent Effect. *J. Power Sources* **2017**, *359*, 198–204. https://doi.org/10.1016/j.jpowsour.2017.05.046.

TOC Online Figure